International Journal of Applied Pharmaceutics

ISSN- 0975-7058 Vol 18, Issue 1, 2026

Original Article

ANTICANCER POTENTIAL OF ULTRASONICATED NANOEMULSION OF NIGELLA SATIVA OIL WITH PHYSICOCHEMICAL CHARACTERIZATION AND CYTOTOXICITY EVALUATION IN MCF-7 BREAST CANCER CELLS

AKASH PODUTWAR, SWATI JAGDALE*

[1]School of Health Sciences and Technology, Department of Pharmaceutical Sciences, Dr. Vishwanath Karad MIT World Peace University, Kothrud-411038, Pune, MH, India

*Corresponding author: Swati Jagdale; *Email: swati.jagdale@mitwpu.edu.in

Received: 07 Aug 2025, Revised and Accepted: 01 Nov 2025

ABSTRACT

Objective: The objective of this study was to develop an ultrasonicated nanoemulsion of *Nigella sativa* (NS) oil and evaluate its anticancer potential through physicochemical characterization and cytotoxicity assessment in MCF-7 breast cancer (BC) cells.

Methods: The nanoemulsion was made utilizing Tween (Tw) 80 and investigated by particle size (PS), zeta potential (ZP), and thermodynamic stability. These parameters were evaluated by assessing physicochemical properties, antioxidant capacity through the DPPH assay, and cytotoxic potential by means of the MTT assay on MCF-7 BC cells.

Results: The finalized batch had a feasible droplet size of 47.09 nm, acceptable stability, and a proficient release profile of the drug in a long-term model (93.74% cumulative release). While nanoemulsion resulted in comparatively lower antioxidant activity than pure NS oil due to encapsulation and demonstrated a significantly lower IC_{50} (1.435±0.148 µl/ml) than paclitaxel (5.317±0.112 µl/ml), and showed enhanced cellular uptake, as confirmed through FITC fluorescence imaging.

Conclusion: The finalized NS oil nanoemulsion demonstrated potent *in vitro* cytotoxicity against MCF-7 cells. However, further *ex-vivo* and *in vivo* investigations are required to confirm its suitability for topical BC therapy.

Keywords: *Nigella sativa*, Breast cancer, MCF-7, DAPI, FITC, Cytotoxicity

DOI: https://dx.doi.org/10.22159/ijap.2026v18i1.56446 Journal homepage: https://innovareacademics.in/journals/index.php/ijap

INTRODUCTION

Breast cancer (BC) is considered the utmost common and deadly disease affecting women worldwide. Chemotherapy, radiation, and hormone therapy have improved patient survival, but their effectiveness is limited by their poor selectivity, systemic toxicity, and resulting multidrug resistance. Moreover, a significant portion of anticancer compounds exhibits poor aqueous solubility and inadequate bioavailability, which deteriorates their performance and produces an excess of side effects [1, 2].

Topical drug delivery has gained popularity as a substitute for the newly popular systemic application technique. It has demonstrated the benefits of localized action, less systemic exposure, and improved patient compliance [3]. However, the solubility and permeability of the active component are crucial to the success of such formulations. These limitations can be addressed by incorporating natural oils with known therapeutic properties, despite their poor water solubility. Essential oils, in particular, represent promising candidates for formulation into advanced drug delivery systems to improve their clinical applicability [4].

Nigella sativa (NS) oil is considered important due to its diverse pharmacological effects, including anticancer activity [5]. Its main bioactive ingredient, thymoquinone, has shown strong anti-inflammatory, anti-proliferative, and antioxidant properties in a diverse cancer cell line, including MCF-7 BC cells. In spite of the above promises, the topical or transdermal clinical translation of NS oil is still limited because of its instability and hydrophobicity [6, 7]. Nanoemulsions provide a suitable platform to address these challenges by improving solubility, enhancing stability, controlling release, and facilitating skin permeation, and also offer several benefits as topical delivery systems. Their nanoscale droplet size enhances drug solubilization and promotes penetration across the stratum corneum. They can provide sustained and controlled drug release, ensure prolonged therapeutic effect while minimizing systemic absorption. Additionally, nanoemulsions facilitate drug localization at the site of application and are relatively simple to prepare and scale up compared to other nanocarrier systems, making them highly suitable for translational applications [8, 9].

To translate the medicinal value of NS oil into practical use, the present research focuses on formulating a nanoemulsion using ultrasonication [10, 11]. The benefits of nanoemulsions include enhanced solubility, better stability, controlled delivery, and skin penetration. A stable NS oil nanoemulsion was formulated for this investigation and described using physicochemical, *in vitro*, and *ex-vivo* analyses. Topical nanoemulsions have been explored as alternatives to systemic chemotherapy. In this study, we developed and evaluated NS oil nanoemulsion for its *in vitro* anticancer activity, while acknowledging that future studies must validate its potential for topical delivery.

MATERIALS AND METHODS

Materials

NS oil was bought from Priest Herbochem (Pune, Maharashtra, India). Tween (Tw) 80, Tw 60, Tw 40, and Tw 20 were procured from Clairofilt India (Mumbai, Maharashtra, India). The MCF-7 cell line has been obtained through the National Centre for Cell Science (NCCS, Pune, Maharashtra, India). Fetal bovine serum (FBS) and Dulbecco's Modified Eagle Medium (DMEM, AT149-1L) were purchased from HiMedia Laboratories (Mumbai, Maharashtra, India). Penicillin-streptomycin was procured from Sigma-Aldrich (Bengaluru, Karnataka, India). Dimethyl sulfoxide (DMSO) was procured from Research-Lab Fine Chem Industries (Mumbai, Maharashtra, India). MTT reagent, APTES, and FITC were purchased from Sisco Research Laboratories (Mumbai, Maharashtra, India). DAPI solution was obtained from ThermoFisher Scientific (Mumbai, Maharashtra, India). Ultrapure water was utilized throughout the experiments unless otherwise specified. Other materials, equipment, and kits are detailed in specific methods.

Method

Oil characterization

GC-MS analysis

The chemical profile of NS oil has been investigated by GC–MS using a formerly reported method with slight alterations [12]. The Shimadzu GCMS-QP2010 Ultra system, prepared with a capillary

column (30 m × 0.25 mm), was utilized for the analysis. The NS oil sample was dissolved in ethyl acetate and derivatized with BSTFA-TMCS before injection. The temperature of the oven program was set to a preliminary temperature of 120 °C, held for 2 min, then boosted at a rate of 10 °C per min to an absolute temperature of 300 °C, where it was held for 20 min. Helium, the carrier gas, was utilized at a split ratio of 10:1 and a flow rate of 1.21 ml/min. The temperature of the injector was 260 °C. m/z 40–650 is the range in which mass spectra were obtained. Compounds were detected by matching the resultant spectra with entries in the NIST mass spectral library.

FTIR analysis

FTIR analysis of NS oil and Tw 80 were carried out using a Shimadzu QATR-S model to identify any significant chemical interactions. The resulting spectra were then plotted and analysed using OriginPro 2025 software.

Emulsification study

An emulsification study was performed using NS oil with non-ionic surfactants for Tw 80, Tw 60, Tw 40, and Tw 20, which are mixed in oil-to-surfactant ratios from 1:9 to 9:1. Ternary phase diagrams were constructed using TernaryPlot.com to identify emulsion regions, and emulsions were prepared using selected compositions from these diagrams. Physical stability was visually assessed after 24 h to check for creaming or phase separation. The surfactant yielding the most stable emulsion was chosen for nanoemulsion development, leading to the preparation of three nanoemulsion batches for further characterization [13, 14]. Tw 80 was selected as the surfactant based on its superior emulsification capacity with NS oil and its pharmaceutical acceptability. Preliminary trials also showed that NS oil alone exhibited emulsifying tendencies when mixed with water.

Preparation of nanoemulsion by ultrasonication

NS oil, Tw 80, and water were used to prepare the nanoemulsion with the composition mentioned in table 1. A measured quantity of water was placed in a beaker, and Tw 80 was added dropwise under constant agitation using a magnetic stirrer to ensure uniform mixing. Subsequently, a measured amount of NS oil was added dropwise to the previous solution to obtain a macroemulsion. The obtained emulsion was sonicated with a probe sonicator (Sonics Vibra-cell, VCX-750) at 20% amplitude and 10 s pulses and 10 s pauses for 1 h. Ultrasonic waves were generated using a 3 mm probe, with an ice bath employed to minimize heat buildup during sonication. The nanoemulsion was eventually acquired after sonication lasted 1 h. The same procedure was used to prepare all three batches [15, 16].

Table 1: Composition of nanoemulsion batches

Batch	NS Oil (%)	Tw 80 (%)	Water (%)
B1	8.00	8.00	84.00
B2	8.00	16.00	76.00
B3	8.00	24.00	68.00

Zeta potential and particle size analysis

Using a Malvern Zetasizer (Nano ZS90), the particle size (PS) and polydispersity index (PDI) have been investigated. Dynamic Light Scattering (DLS) is used to determine the droplet size. The average size of droplet, ZP, and PDI were recorded for all 3 batches.

Turbidity analysis

Prepared nanoemulsion was diluted 100 times using double-distilled water and examined using a UV-VIS Spectrophotometer (Shimadzu, UV-1780) at 650 nm, and % transmittance was calculated keeping water as a blank [17].

Thermodynamic stability studies

Nanoemulsion batches (B1, B2, B3) were attributed to centrifugation at 5000 rpm for 1 h, followed by six heating–cooling cycles (8 °C and 40 °C, 48 h each), and three freeze–thaw cycles (-25 °C to 25 °C, 24 h each). Visual inspection and DLS measurements after each cycle were used to evaluate phase separation, clarity, PDI, PS, and ZP, thereby assessing stability [18].

Intermediate stability studies

Prepared nanoemulsion batches (B1, B2, B3) were also subjected to an intermediate stability study as per ICH guidelines. Formulations were stored at 30±2 °C and 65±5% RH for 180 days. Samples were analysed using a Malvern Zetasizer (Nano ZS90) with DLS to determine PS, PDI, and droplet size [19].

Drug content

The drug content of the batch B3 was evaluated using UV–Visible spectrophotometry. To ensure complete solubilization of the drug, a measured volume of nanoemulsion was diluted with ethanol to a total of 10 ml, effectively disrupting the emulsion matrix and promoting efficient drug extraction. The mixture was then magnetically stirred for 30 min at ambient temperature to facilitate thorough mixing and dissolution. Following this, the sample was explored using a UV–Visible spectrophotometer at a 257.5 nm of wavelength, with ethanol utilized as the blank [20].

***In vitro* drug release by dialysis membrane**

The *in vitro* drug release profile was assessed using the dialysis membrane diffusion method with pH 7.4 phosphate buffer as the release medium. Before the experiment, dialysis membranes (MWCO 12,000–14,000 Da; HiMedia, Mumbai) were pre-soaked in the buffer for 12 h to achieve adequate hydration. A 2 ml aliquot of the nanoemulsion batch B3 was placed inside the dialysis bag and deep in 100 ml of dissolution medium sustained at 37±0.5 °C with constant stirring at 50 rpm. The release medium volume was selected to maintain sink conditions throughout the study, based on the reported solubility of thymoquinone (0.5 mg/ml) in phosphate buffer (pH 7.4) [21]. The chosen 1:50 (v/v) nanoemulsion-to-medium ratio ensured sufficient solvent capacity for complete diffusion of the released drug, in accordance with regulatory recommendations for *in vitro* release testing [22, 23]. At fixed intervals (1, 2, 3, 4, 5, 6, 7, 8 h), 1 ml samples were withdrawn and substituted with fresh buffer to preserve sink circumstances. Drug release was quantified using a UV–VIS spectrophotometer at 257.5 nm. The cumulative release data were fitted to several kinetic models, comprising first-order, zero-order, Higuchi-Matrix, Korsmeyer–Peppas, and Hixson–Crowell, to elucidate the release mechanism. The model showing the highest R^2 was considered the best fit [24, 25].

DPPH scavenging assay

The antioxidant activity of NS oil and the nanoemulsion batch B3 was estimated by using the DPPH radical scavenging assay, with minor modifications to a previously established method [26]. Working solutions were prepared by diluting 0.8 ml of NS oil and 0.8 ml of batch B3 separately in 10 ml of ethanol. 0.8 g of ascorbic acid was dispersed in 10 ml of distilled water to prepare an ascorbic acid solution, which served as a positive control. 6 mg of DPPH were dissolved in 100 ml of methanol to create a new DPPH reagent having a concentration of 60 µg/ml. To perform the assay, 1 ml of each test solution at varying concentrations was mixed in a 1:1 ratio with 1 ml of DPPH solution in clean, labelled test tubes. The assay mixtures were kept in the dark for 20 min at room temperature to facilitate the reaction with DPPH radicals. Following incubation, the absorbance of each sample was measured at 517 nm using a UV-

Visible spectrophotometer. The negative control was a methanolic DPPH solution without any test sample, as well as a positive control, ascorbic acid. Percentage scavenging activity was determined as follows:

$$\% \text{ Scavenging Activity} = \frac{(\text{Abs control} - \text{Abs sample})}{\text{Abs control}} \times 100 \ldots\ldots\ldots (1)$$

In this case, the absorbance of the DPPH solution alone is the Abs control, while the absorbance of the sample is the Abs sample.

Cellular morphological analysis

Cell morphology was assessed using brightfield microscopy to examine the impact of batch B3 on MCF-7 cells. The cells were incubated with both and without batch B3 for 24 h. After incubation, a digital camera-equipped optical microscope was used to take brightfield images, utilizing a 100x objective for fine-grained visualization.

Cytotoxicity study

MTT assay was conducted on the MCF-7 cell line to determine the cytotoxic ability of the nanoemulsion batch B3 [27]. The standard protocol was followed in the performance of the assay. The MCF-7 cells (10,000 cells/well) were plated in a 96-well plate and incubated at 37 ºC with 5% CO_2 in DMEM F12 media consisting of 10% fetal bovine serum (FBS) along with Penicillin-Streptomycin (1% solution). The nanoemulsion batch B3 was treated to the cells after 24 h of incubation in various doses. To get the necessary concentrations, a stock solution of batch B3 and paclitaxel (853.9 g/mol) was made in dimethyl sulfoxide (DMSO, 0.5%) and then further diluted in incomplete culture media (without FBS). For conversion to standard concentration units, the paclitaxel stock solution (50 µM = 50,000 nM) was prepared in 0.5% DMSO, and equivalent concentrations in µl**/ml were derived using the dilution relationship:

$$\text{Volume added } (\mu l) = \frac{\text{Final conc (nM)} \times \text{Final volume (µl)}}{\text{Stock conc (nM)}} \ldots\ldots (2)$$

$$\mu l/ml = \frac{\text{Volume added (µl)}}{\text{Final Volume (ml)}} \ldots\ldots (3)$$

Untreated cells served as the control, while wells without MTT solution were used as blanks. After being exposed for 24 h, each well received 5 mg/ml of MTT solution, and the plates were kept for incubation for 2 h. After carefully removing the supernatant, 100 µl of DMSO was used to solubilize the formazan crystals. An ELISA plate reader was used to detect absorbance at 540 nm. The percentage of viable cells was assessed using the formula:

$$\% \text{ Viable cells } = \frac{A_{test}}{A_{Control}} \times 100 \ldots\ldots (4)$$

Nuclear morphological analysis DAPI staining

MCF-7 cells were put onto ultraclean coverslips in 6-well plates at a population of 5,000–10,000 cells/well. Each well was treated with 200 µl of APTES (3-aminopropyltriethoxysilane, 1% v/v) for 1 h at room temperature. Excess APTES was discarded, and wells were rinsed twice with complete medium. At 90% confluency, cells were harvested, seeded, and incubated for 24 h at 37 °C in 5% CO_2. After incubation, cells were incubated for a further 24 h in a new medium that contained the appropriate quantity of batch B3 and FITC (fluorescein isothiocyanate, 1 µl/ml). Cells were then fixed for 20 min with 1 ml of 3% paraformaldehyde and rinsed with sterile phosphate-buffered saline. The addition of DAPI solution (4′,6-diamidino-2-phenylindole, 100 µl, 1 µg/ml) was followed by a PBS wash after 30 min of incubation. An inverted laser scanning confocal microscope (ZEISS, LSM 900) was used to view coverslips mounted on pristine glass slides under DAPI, FITC, and merged channels. Following FITC incubation, wells were washed repeatedly with PBS until no residual fluorescence was detectable in the wash solution, confirming removal of unbound FITC and stability of conjugation mean fluorescence intensity was quantified using ImageJ (Version 1.54d), background-corrected using the control group, and normalized to determine APTES–FITC conjugation efficiency [28, 29].

RESULTS

Oil characterization and pre-formulation studies

GC-MS analysis

GC–MS analysis of the NS oil confirmed the occurrence of 17 volatile constituents (fig. 1), primarily consisting of terpenes. The sample also contained several minor constituents such as Sabinene, β-Pinene, γ-Terpinene, and Limonene oxide, contributing to the oil's complex phytochemical profile.

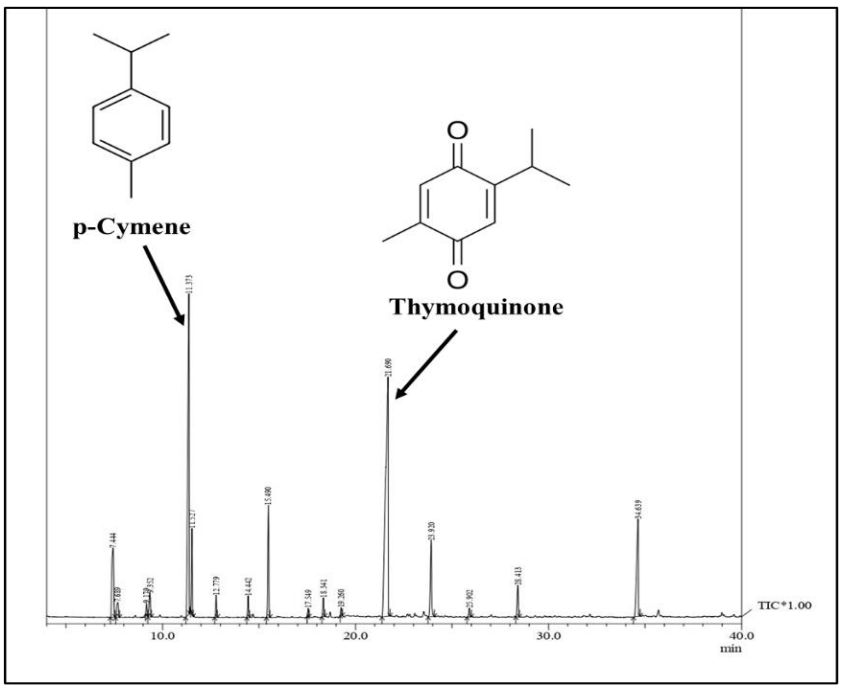

Fig. 1: GC-MS chromatogram of NS oil, the major compound was thymoquinone (35.51%), followed by p-Cymene (23.43%), and others as mentioned in table 2

Table 2: Composition of NS oil by GC-MS analysis, along with their retention time and percentage area

Peak	R. Time	% Area	Names of compounds
1	7.444	7.04	α-Thujene
2	7.689	1.47	Bicyclo [3.1.1] Hept-2-Ene,2,6,6-Trimethyl
3	9.179	0.60	Sabinene
4	9.352	1.64	β-Pinene
5	11.373	23.43	ρ-Cymene
6	11.527	3.64	Limonene
7	12.779	1.01	γ-Terpinene
8	14.442	1.03	(1r,4r,5s)-1-Isopropyl-4-Methoxy-4-methylbicyclo-[3.1.0]-hexane
9	15.490	6.06	(1r,4r,5s)-1-Isopropyl-4-Methoxy-4-Methylbicyclo-[3.1.0]-hexane
10	17.549	0.42	Cis-LimoneneOxide
11	18.341	1.04	3-Cyclohexen-1-ol,4-Methyl-1-(1-METHYLETHYL)
12	19.260	0.40	Cis-, Para-Mentha-2,8-Dien-1-ol
13	21.690	35.51	Thymoquinone
14	23.920	5.20	Carvacrol
15	25.902	0.53	Tricyclo-[5.4.0.0(2,8)]-Undec-9-Ene-2,6,6,9-tetramethyl
16	28.413	1.96	(+)-Longifolene
17	34.639	9.01	P-Cymene-2,5-Diol
		100.00	

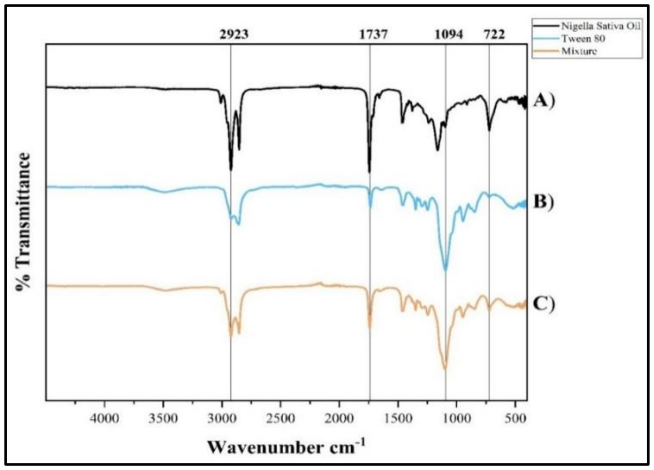

Fig. 2: FTIR spectra of A) NS oil, B) Tw 80, and C) physical mixture of both

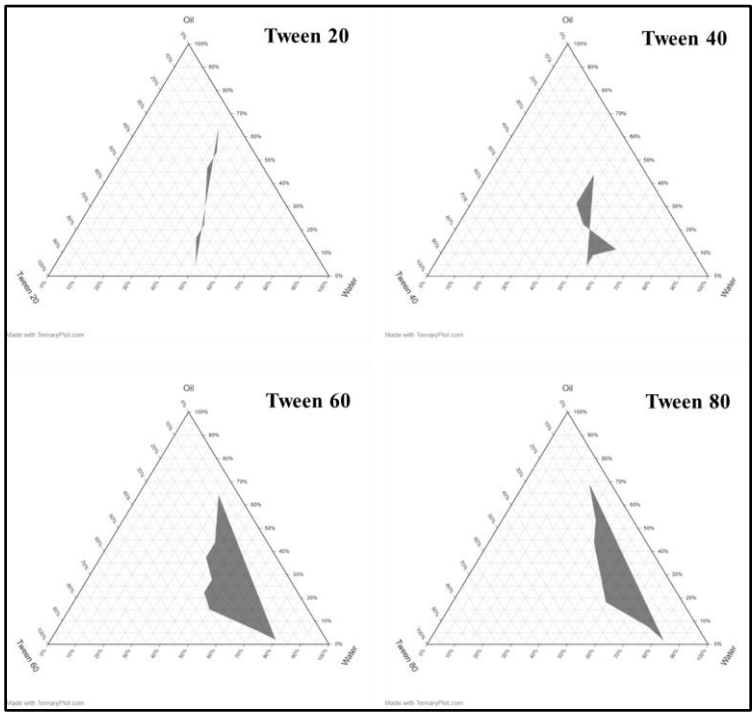

Fig. 3: Ternary plot diagrams

FTIR analysis

The FTIR spectra show distinct characteristic peaks for NS oil, Tw 80, and their mixture. NS oil exhibits prominent absorption bands at 2923 cm^{-1} (C–H stretching of aliphatic chains), 1737 cm^{-1} (C=O stretching of esters), 1094 cm^{-1} (C–O stretching), and 722 cm^{-1} (–$(CH_2)_n$– rocking) [12]. Tw 80 shows similar peaks corresponding to its own functional groups [30]. The mixture spectrum displays all these characteristic peaks without notable shifts or the formation of new peaks (fig. 2).

Emulsification study

Ternary phase diagrams for each surfactant, Tw 80, Tw 60, Tw 40, and Tw 20, were constructed using Ternaryplot. com, as illustrated in fig. 3. The shaded regions in each diagram represent the compositional zones capable of forming nanoemulsions. Random formulations were selected from these regions to evaluate emulsion formation and stability.

After 24 h of observation, emulsions prepared using Tw 60, Tw 40, and Tw 20 exhibited phase separation, indicating physical instability. In contrast, the emulsions formulated with Tw 80 remained physically stable, showing no signs of creaming or phase separation. Therefore, Tw 80 was selected for the nanoemulsion formulation. Fig. 4 illustrates the freshly prepared nanoemulsion batches developed using Tw 80.

Zeta potential and particle size

The ZP, PDI, and PS of the formulated nanoemulsions were analysed for three different batches before thermodynamic stability, as reported in table 3.

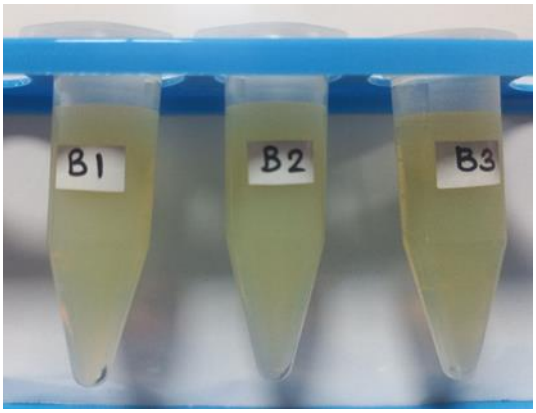

Fig. 4: Nanoemulsion batches

Table 3: ZP, PS, and PDI of all three batches before and after thermodynamic stability, and after 6 mo of stability studies

Batches	Before thermodynamic stability			After thermodynamic stability			Intermediate stability studies		
	ZP (mV)	PS (nm)	PDI	ZP (mV)	PS (nm)	PDI	ZP (mV)	PS (nm)	PDI
B1	-16.2	56.53	0.398	-2.61	178.5	0.063	-4.95	139.6	0.317
B2	-16.8	68.48	0.525	-11.3	156.5	0.175	-2.55	131.6	0.283
B3	-9.49	47.09	0.401	-8.27	79.70	0.224	-2.53	77.70	0.201

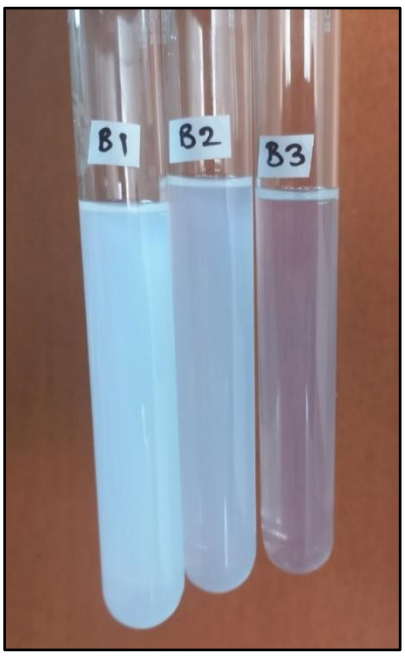

Fig. 5: Turbidity analysis of nanoemulsion batches B1, B2, and B3 captured after 100x dilution of each batch

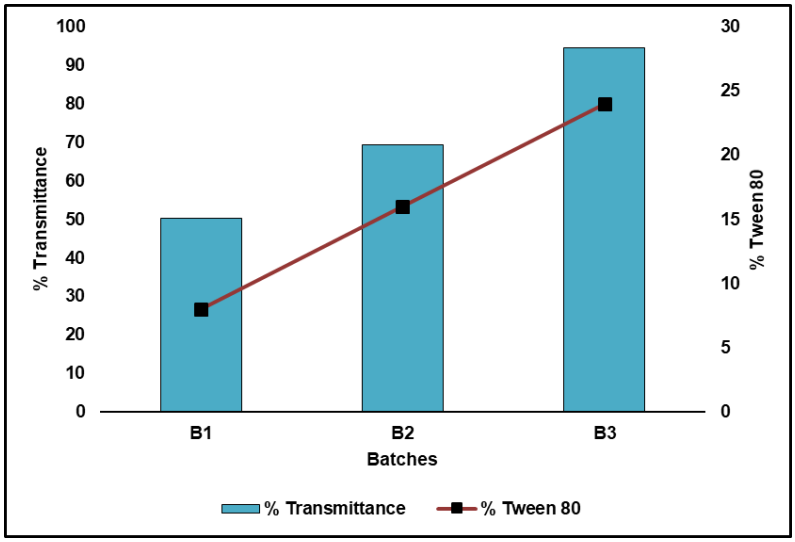

Fig. 6: Influence of Tw 80 on the % transmittance of nanoemulsion batch B1, B2 and B3

Turbidity analysis

All of the prepared batches' turbidity was quantified by UV-VIS spectroscopy at 650 nm. Fig. 5 illustrates the turbidity of all three batches after a 100x dilution. Fig. 6 illustrates the inverse relationship between the turbidity measurements and the surfactant concentration used in each batch.

Thermodynamic stability studies

All batches underwent centrifugation, heating-cooling, and freeze-thaw cycles. There was no phase separation throughout the heating-cooling or centrifugation cycles. However, freeze-thaw cycles caused opacification in B1 and B2, while B3 remained clear, as shown in fig. 7.

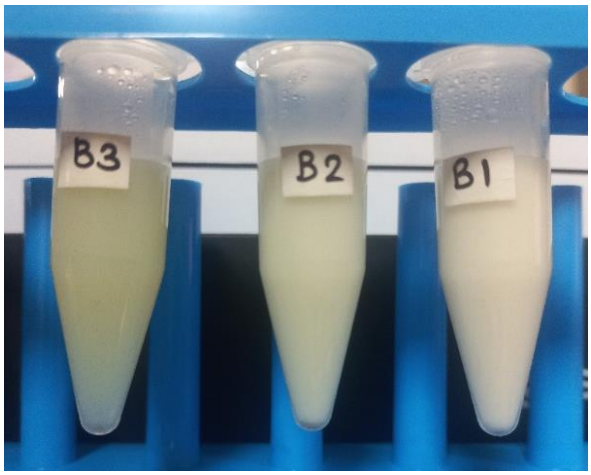

Fig. 7: Image captured after thermodynamic stability of nanoemulsion batches B1, B2, and B3

Post thermodynamic stability studies PS, ZP, and PDI of all three batches were analysed as reported in table 3. These results confirm that batch B3 has relatively more stability compared to batches B1 and B2.

Intermediate stability studies

After completion of 180 d, all three batches were analysed for PS, ZP, and PDI, and are given in table 3. The intermediate stability study also confirms that batch B3 is more stable compared to batches B1 and B2.

Drug content

Batches B1 and B2 were found to be unstable in the thermodynamic stability studies; therefore, batch B3 was selected for further evaluation. The drug content of batch B3 was evaluated using UV-Visible spectrophotometry at 257.5 nm and was found to be 72.12 ± 3.1%. The consistency among triplicate samples reflects uniform drug distribution and reproducibility of the formulation.

In vitro drug release

NS oil and batch B3 were tested for *in vitro* drug release profiles using a dialysis membrane diffusion method in phosphate buffer (pH 7.4). The collective percentage drug release was deliberate and plotted against time, as shown in fig. 8. The results showed a significantly enhanced drug release from batch B3 compared to the plain NS oil. After 8 h, batch B3 exhibited a cumulative drug release of 93.74%, whereas NS oil showed only 43.55% release.

The *in vitro* drug release study of batch B3 revealed a sustained release profile, with 93.74% cumulative drug release observed at 8 h. The release data were fitted to several kinetic models, such as zero-order, first-order, Higuchi, Korsmeyer–Peppas, and Hixon-Crowell equations, to comprehend the drug release process.

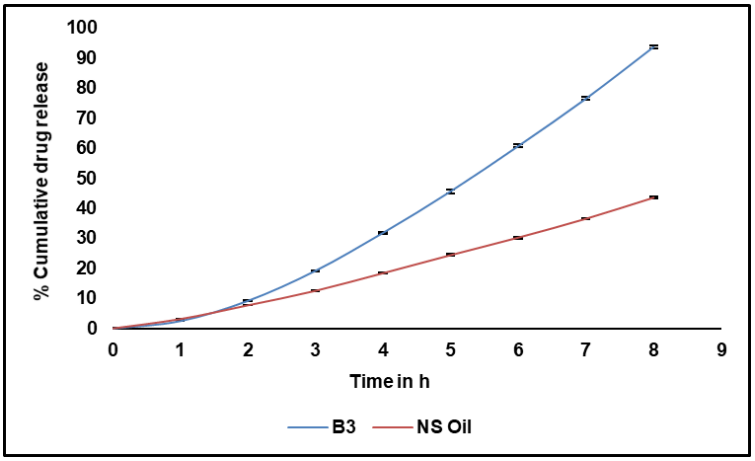

Fig. 8: Percentage cumulative drug release of pure NS oil vs batch B3 in phosphate buffer pH 7.4; (n=3)

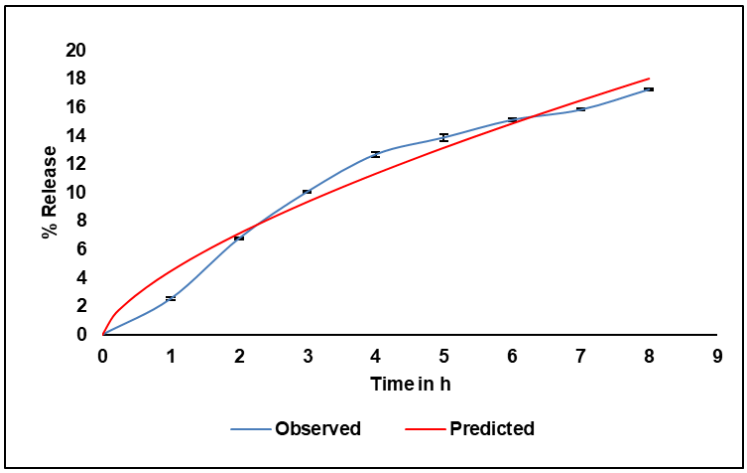

Fig. 9: Release kinetics best fit the Korsmeyer–Peppas model, with an R^2 value of 0.9737; (n=3)

Among these, the Korsmeyer–Peppas model showed the best fit, exhibiting a high correlation coefficient (R^2= 0.9737), indicating that this model most accurately described the drug release behaviour (fig. 9). The model is expressed as:

$$F = K_{kp} \times t^n \ldots\ldots\ldots\ldots (3)$$

Where n is the release exponent, K_{kp} is the release rate constant, and F is the percentage of medication released at time t. The calculated values were K_{kp}= 4.487 and n= 0.669.

DPPH radical scavenging assay

The antioxidant potential of NS oil and batch B3 was assessed using the DPPH radical scavenging assay, with ascorbic acid as a standard. The percentage scavenging activity was calculated at the range of concentrations from 0.1 to 0.5 µg/ml, and results are presented in fig. 10. Ascorbic acid demonstrated the highest scavenging activity, increasing from 65.9% to 95.6% across the tested concentrations. NS oil showed moderate activity, ranging from 55.3% to 78.2%, while batch B3 exhibited the lowest activity, from 54.0% to 56.6%.

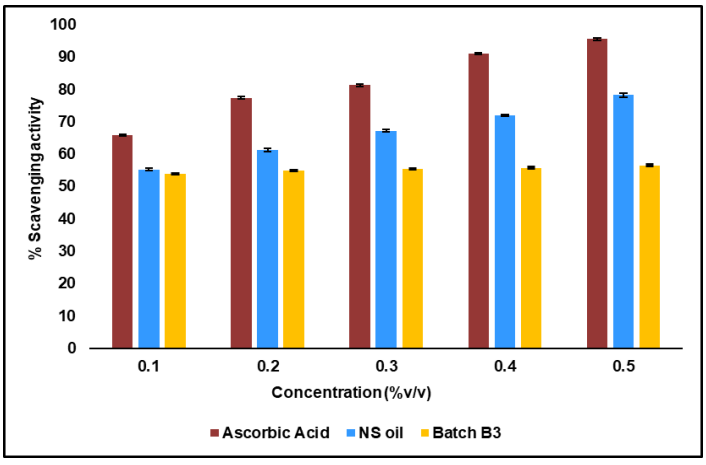

Fig. 10: Percentage scavenging activity versus concentration for ascorbic acid, NS oil, and the prepared nanoemulsion batch B3; (n=3)

Cellular morphological analysis

The morphological variations in MCF-7 cells after treatment for 24 h with batch B3 were observed under a brightfield microscope (fig.11). Untreated control cells (fig.11A) exhibited a characteristic epithelial-like, spindle-shaped morphology, with intact cell membranes and high confluency, indicating normal growth. In contrast, exposed cells (fig.11B) showed membrane shrinkage, cytoplasmic condensation, and loss of adherence. Additionally, an increased presence of round, detached, and floating cells was observed.

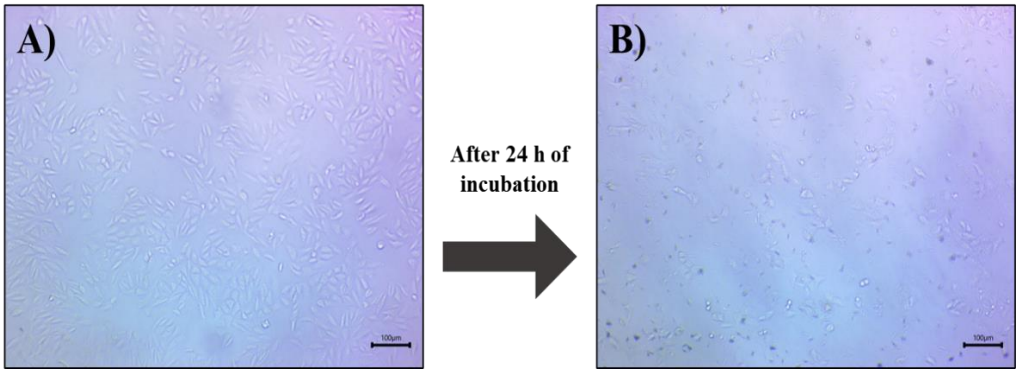

Fig. 11: Brightfield microscopic images of MCF-7 cells after 24 h of incubation: (A) untreated (control) and (B) treated with nanoemulsion batch B3. (Scale-100 µm)

Cytotoxicity study

The cytotoxic potential of batch B3 was evaluated using the MTT assay on MCF-7 BC cells. Cells were exposed to varying concentrations of the nanoemulsion and standard drug (paclitaxel), as shown in fig. 12, and the IC_{50} values were determined. The results revealed that batch B3 exhibited a higher cytotoxic effect compared to paclitaxel.

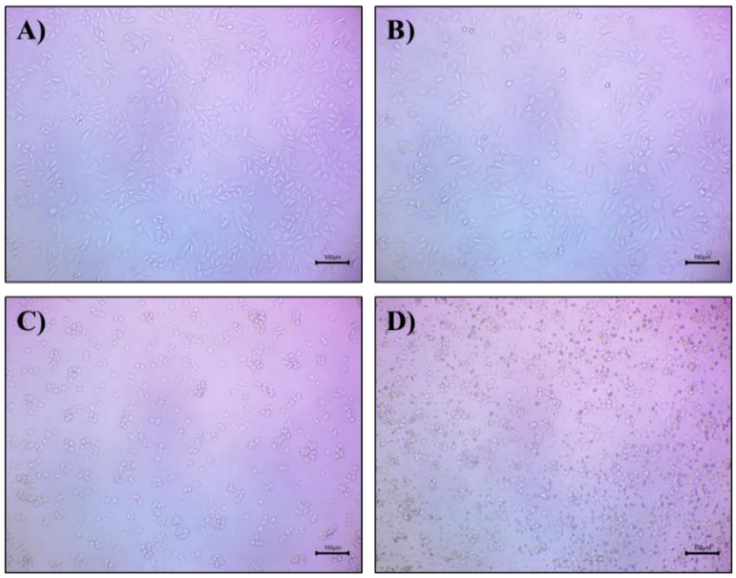

Fig. 12: Microscopic images of MCF-7 cells treated with nanoemulsion batch B3 at varying concentrations: (A) control, (B) 0.78125 µl/ml, (C) 6.25 µl/ml, and (D) 50 µl/ml. (Scale-100 µm)

The IC_{50} value of batch B3 was found to be 1.435±0.148 µl/ml, whereas paclitaxel exhibited an IC_{50} value of 5.317±0.112 µl**/ml, corresponding to 265.8±0.11 nM, based on its molecular weight (853.9 g/mol) and stock concentration. Fig. 13 shows the comparative % cell viability for the prepared nanoemulsion and paclitaxel.

Cellular and nuclear analysis via FITC and DAPI staining

Cellular uptake investigation via FITC imaging

The ability of the synthesized batch B3 to penetrate and be internalized by MCF-7 cells was evaluated using FITC-based fluorescence imaging. FITC-labelled formulations were incubated with MCF-7 cells for 24 h, and the intracellular fluorescence intensity was analysed using ImageJ software. Microscopic images showed that the FITC intensity in cells treated with batch B3 (fig. 14H) was significantly higher than that treated with Paclitaxel (fig. 14E) and comparable to the control group (fig. 14B) (untreated FITC exposure).

Quantitative fluorescence analysis revealed that APTES–FITC conjugation efficiency was highest for NS NE B3 (100%) compared with Paclitaxel (25%), after background correction against the control group. This confirms successful APTES–FITC functionalization and supports the superior cellular uptake of B3 observed under confocal microscopy. The mean FITC intensity for the control, paclitaxel, and batch B3 groups was 65.93, 46.65, and 63.69, respectively. When normalized to the control (considered 100%), the relative FITC intensities were 96.59% for batch B3 and 70.76% for Paclitaxel.

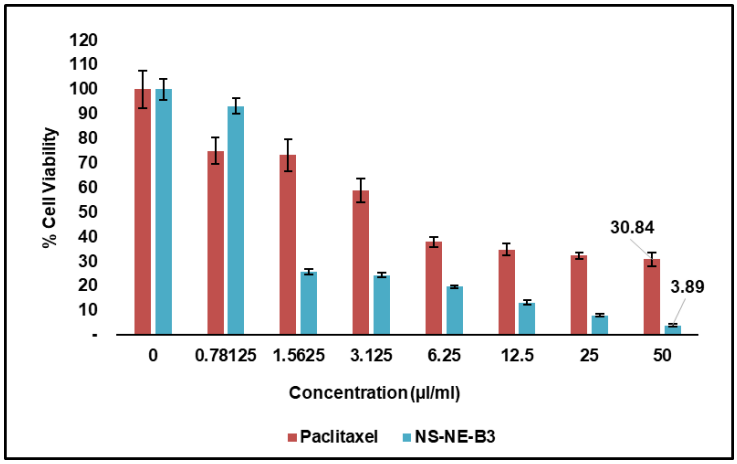

Fig. 13: Percentage cell viability and cytotoxicity of nanoemulsion batch B3 and standard paclitaxel against MCF-7 BC cells across concentrations ranging from 0 to 50 µl/ml; (n=4)

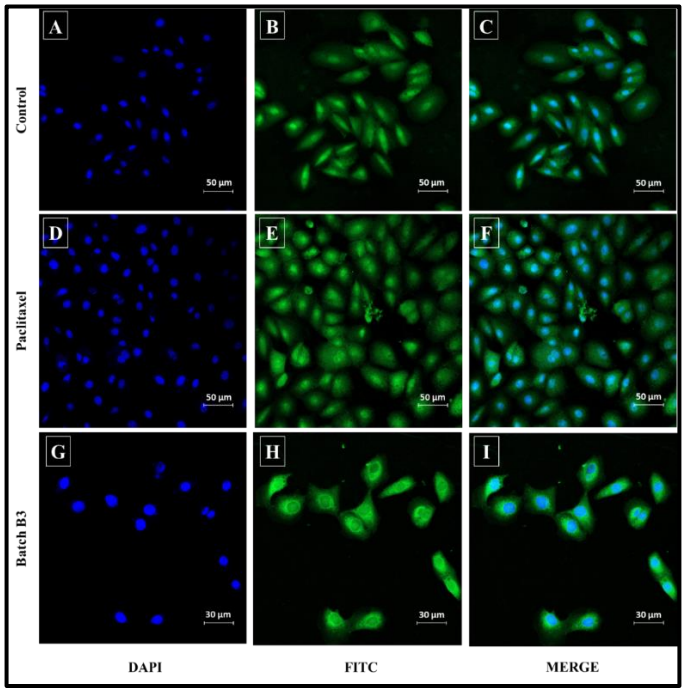

Fig. 14: FITC and DAPI staining of MCF-7 cancer cells captured by confocal microscopy. Images A, B, and C represent the control group; images D, E, and F show cells treated with paclitaxel; and images G, H, and I show cells treated with nanoemulsion batch B3

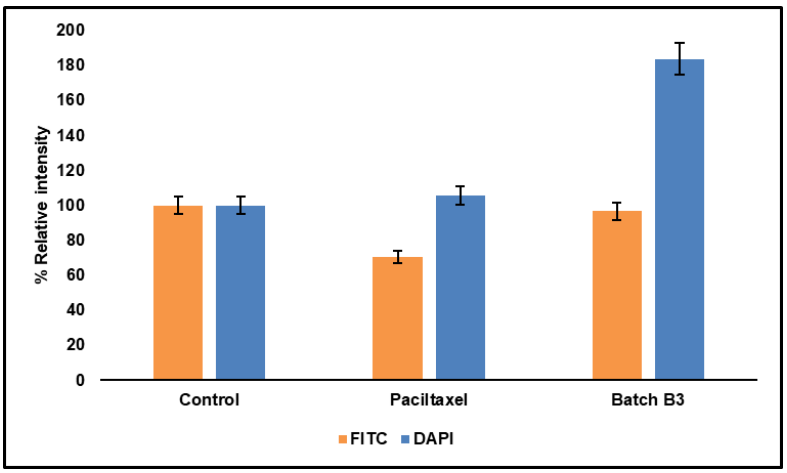

Fig. 15: Percentage relative intensity graph for FITC and DAPI; (n=3)

Nuclear analysis by DAPI staining (Cell apoptosis assay)

DAPI staining was employed to examine nuclear morphology and evaluate apoptosis in MCF-7 cells treated with batch B3, Paclitaxel, and control. MCF-7 cells were stained after 24 h of treatment, and images were captured using confocal microscopy. Untreated control cells exhibited normal nuclear morphology with uniform fluorescence, indicating intact chromatin. Cells treated with paclitaxel displayed slightly increased DAPI fluorescence, while those exposed to batch B3 exhibited significantly brighter nuclear staining (fig. 14). Quantitative intensity analysis showed mean values of 122.27 for control, 129.15 for Paclitaxel, and 224.72 for batch B3. When normalized, batch B3 group showed a 183.79% increase in nuclear intensity relative to control, while paclitaxel-treated cells showed a modest 105.63% increase, as depicted in fig. 15.

DISCUSSION

Nanoemulsions prepared with natural oils have gained attention recently as nanoemulsions increase the solubility and stability of pure natural oils like NS, which is more beneficial in the case of treatment options for diseases like BC. This study develops a nanoemulsion of NS oil and evaluates its anticancer, antioxidant, cellular, and nuclear uptake in the MCF-7 cell line.

In this study, a surfactant-only system was adopted, as preliminary trials indicated that NS oil itself showed emulsifying tendencies when mixed with water. Literature also supports the feasibility of co-surfactant-free emulsions, where intrinsic oil components and suitable surfactants are sufficient for stable formulation [31, 32]. Moreover, co-surfactants have been reported to potentially destabilize emulsions upon dilution due to phase partitioning [33]. Therefore, Tw 80 alone was used to achieve a stable nanoemulsion while minimizing possible drawbacks associated with co-surfactants.

The GC-MS revealed that the composition of NS was rich in monoterpenes and phenolic derivatives, indicating a strong potential for pharmacological applications because of their known antioxidant and anti-inflammatory properties. A. Piras *et al.* have previously reported on all of the main components [34]. The presence of Thymoquinone as the principal compound highlights the therapeutic relevance and quality of the NS oil used. The diversity of compounds identified supports its suitability for formulation into advanced drug delivery systems, such as nanoemulsions, to enhance bioavailability and therapeutic action.

In FTIR studies, the absence of shifts or new peaks confirms the absence of chemical interactions and suggests a physical blending of NS oil and Tw 80. Reduced turbidity and correspondingly increased transmittance are the results of higher surfactant concentrations [35]. This effect demonstrated the property of surfactant at higher concentrations to significantly reduce droplet size. The findings suggest that increasing the concentration of Tw 80 in the nanoemulsion formulation can effectively reduce droplet size and turbidity. The observed colour change during thermodynamic stability in the nanoemulsions indicates an increase in PS due to Ostwald ripening, a common phenomenon in nanoemulsions [36]. After the intermediate stability study, all three batches showed an increase in PS, most likely due to Ostwald ripening. This can be attributed to the general phenomenon wherein increasing PS leads to a reduction in ZP, as the decrease in surface area reduces the availability of surface charges [37]. Additionally, hydrogen bonding between water molecules and the oxyethylene groups of Tw 80 may promote selective hydroxyl ion adsorption at the oil–water interface, leading to a negative charge [38].

The level of drug content indicates acceptable incorporation of the active compound into the nanoemulsion system and suggests that the formulation process effectively solubilized and entrapped the drug, making it suitable for topical or transdermal delivery [39]. The use of magnetic stirring and ethanol dilution may have further contributed to improved dispersion and accurate quantification.

The substantial improvement in drug release from the nanoemulsion can be attributed to its smaller droplet size and improved surface area, which facilitates faster diffusion across the dialysis membrane. An *n* value ranging from 0.45 to 0.89 indicates non-Fickian (anomalous) diffusion, implying that drug release is controlled by both diffusion and erosion mechanisms [40]. The observed controlled and sustained release behaviour is beneficial to maintain therapeutic drug concentrations over a prolonged period, potentially reducing dosing frequency and enhancing patient compliance.

The antioxidant activity of the nanoemulsion (B3), as measured by the DPPH assay, was found to be slightly lower than that of pure NS oil. This apparent reduction can be attributed to the encapsulation of bioactive compounds such as thymoquinone within the oil droplets, which restricts their immediate interaction with DPPH radicals in the assay medium. Similar findings have been reported in other encapsulation studies, where nano-emulsified plant extracts exhibited reduced instantaneous radical scavenging activity but demonstrated enhanced oxidative stability and preservation of bioactivity over time. Sánchez-López *et al.* emphasized that encapsulation improves stability and provides controlled release of antioxidant molecules, thereby sustaining activity under physiological conditions [41]. Likewise, Medina-Pérez *et al.* reported that encapsulation of cactus fruit extracts preserved phenolic compounds and antioxidant capacity during storage and simulated gastrointestinal digestion, despite lower initial DPPH values compared to the free extract [42]. Thus, while batch B3 exhibited moderately reduced immediate DPPH scavenging, the nanoemulsion system is expected to protect thymoquinone against degradation and ensure prolonged antioxidant functionality. This highlights a limitation of the DPPH assay, which primarily reflects short-term radical scavenging, rather than the long-term antioxidant efficacy of encapsulated formulations.

The observed morphological changes in treated cells suggest cytotoxic effects. The severity of these changes intensified with increasing treatment concentrations, confirming the impact of the nanoemulsion formulation on MCF-7 cell viability [43]. These features indicate possible induction of apoptosis or necrosis. The IC_{50} value is the concentration of a compound required to reduce cell viability to 50%, demonstrating the potency of batch B3 in inhibiting MCF-7 cell proliferation. The MTT assay confirmed a dose-dependent decrease in cell viability, indicating strong anti-proliferative activity [35].

The results from FITC imaging confirm that batch B3 exhibits better cellular uptake than Paclitaxel, likely due to its nano-sized droplets and enhanced permeability. The improved fluorescence intensity indicates effective internalization of the nanoemulsion formulation into MCF-7 cells, supporting its potential as an efficient delivery system in BC therapy. DAPI binds strongly to DNA, and changes in nuclear fluorescence intensity can reflect chromatin condensation or DNA fragmentation, hallmarks of apoptotic cell death. The significantly brighter nuclear staining in batch B3-treated cells indicates condensed chromatin and possible apoptotic activity. These results suggest that batch B3 may exert stronger apoptotic effects on MCF-7 cells than standard Paclitaxel, potentially due to improved nuclear delivery of active agents or enhanced cellular interaction. The high DAPI intensity supports the capability of the formulation to induce DNA-related changes leading to cell death. Also, the higher FITC conjugation efficiency observed with B3 can be attributed to its nano-sized droplets, which provide a significantly larger surface area for APTES functionalization compared with bulk paclitaxel particles. This enhanced surface availability facilitates more effective FITC labelling and may contribute to the improved cellular uptake observed. While DAPI and FITC staining provide useful preliminary evidence of nuclear condensation, fragmentation, and cellular uptake associated with apoptosis, these findings should be interpreted as indicative rather than confirmatory. Such assays remain valuable in early-stage evaluations to demonstrate apoptosis-related features, which can be further validated through advanced mechanistic studies in future work.

It is important to note that Tw 80 was selected as the surfactant in the present nanoemulsion system due to its established pharmaceutical acceptability and safety profile. Tw 80 is designated as GRAS and has been widely used in parenteral, oral, and topical formulations at low concentrations. Several reports have demonstrated that Tw 80 alone

does not induce significant cytotoxicity in MCF-7 cells or other cancer models. Mokhtary *et al.* reported that Tw 80-based blank vesicles exhibited no cytotoxic effect on MCF-7 cells and even promoted monocyte growth [44]. Similarly, Chang *et al.* showed that Tw 20 and Tw 80 were non-toxic, and Ghosh *et al.* identified Tw 80 as the least cytotoxic surfactant among those tested [28, 45]. Therefore, the cytotoxic and cellular uptake effects observed in our study can be attributed predominantly to the bioactive constituents of NS oil, particularly thymoquinone, rather than the surfactant or sonication process. However, we acknowledge that a blank (Tw 80+water) nanoemulsion control was not included in this study, and we have identified this as a limitation. Future studies will incorporate surfactant-only controls to further confirm the specificity of NS oil-mediated cytotoxicity.

The developed nanoemulsion formulations of NS oil were successfully evaluated. Further improvements, particularly in enhancing the antioxidant potential and ensuring formulation robustness, are essential to maintain consistency and efficacy. The nanoemulsion exhibited strong *in vitro* cytotoxicity and cellular uptake, supporting its promise as a drug delivery system. Nevertheless, the lack of *ex-vivo* skin permeation and dermatokinetics studies is a limitation of the present work, and future studies are warranted to validate its topical applicability.

CONCLUSION

In conclusion, this study successfully developed and characterized a stable nanoemulsion of NS oil (batch B3) using ultrasonication for potential localized BC therapy. The finalised nanoemulsion formulation exhibited favourable physicochemical properties, including small droplet size, acceptable ZP, and robust thermodynamic stability. Batch B3 demonstrated sustained drug release (93.74% over 8 h) following the Korsmeyer-Peppas model, potent cytotoxicity against MCF-7 cells (IC_{50} = 1.435 µl/ml), and enhanced cellular uptake compared to paclitaxel, indicating superior *in vitro* efficacy. These findings highlight the nanoemulsion's effectiveness in terms of *in vitro* cytotoxicity and cellular uptake. The incorporation of Tw 80 contributed to improved dispersion and stability of the formulation. However, while the *in vitro* results are encouraging, the absence of *ex-vivo* skin permeation and dermatokinetics studies represents a limitation of the present work. Future investigations, including permeation, local tissue retention, and irritation assessments, are required to validate its applicability for topical delivery. Overall, the developed nanoemulsion induced apoptosis-related changes more prominently than paclitaxel, underscoring its promise as a BC therapy, while recognizing the need for further mechanistic validation.

FUNDING

Nil

ABBREVIATIONS

BC: Breast cancer, NS: *Nigella sativa,* Tw: Tween, PS: Particle Size, ZP: Zeta Potential

AUTHORS CONTRIBUTIONS

AP conceptualized and designed the study, acquired the data, performed data analysis and interpretation, and drafted the manuscript. SJ contributed to data interpretation, provided critical revisions, assisted in statistical analysis, and offered administrative and technical supervision. Both authors reviewed and approved the final version of the manuscript before submission.

CONFLICT OF INTERESTS

Declared none

REFERENCES

1. Kaur R, Bhardwaj A, Gupta S. Cancer treatment therapies: traditional to modern approaches to combat cancers. Mol Biol Rep. 2023;50(11):9663-76. doi: 10.1007/s11033-023-08809-3, PMID 37828275.
2. Kumar A. Comprehensive review on etiopathogenesis, treatment and emerging therapies of breast cancer. Asian J Pharm Clin Res. 2021;14(8):20-33. doi: 10.22159/ajpcr.2021.v14i8.41974.
3. Ioele G, Chieffallo M, Occhiuzzi MA, De Luca M, Garofalo A, Ragno G. Anticancer drugs: recent strategies to improve stability profile, pharmacokinetic and pharmacodynamic properties. Molecules. 2022;27(17):5436. doi: 10.3390/molecules27175436, PMID 36080203.
4. Shah SW, Li X, Yuan H, Shen H, Quan S, Pan G. Innovative transdermal drug delivery systems: benefits challenges and emerging application. BME Mat. 2025. p. 1-31. doi: 10.1002/bmm2.70001.
5. Majeed A, Muhammad Z, Ahmad H, Rehmanullah, Hayat SS, Inayat N. Nigella sativa L.: uses in traditional and contemporary medicines an overview. Acta Ecol Sin. 2021;41(4):253-8. doi: 10.1016/j.chnaes.2020.02.001.
6. Fomina DV, Abdullaev SA, Raeva NF, Zasukhina GD. A component of the *Nigella sativa* plant as a radioprotector and antitumor drug. Biol Bull. 2024;51(12):3696-700. doi: 10.1134/S1062359024701917.
7. Bruno MC, Gagliardi A, Mancuso A, Barone A, Tarsitano M, Cosco D. Oleic acid-based vesicular nanocarriers for topical delivery of the natural drug thymoquinone: improvement of anti-inflammatory activity. J Control Release. 2022;352:74-86. doi: 10.1016/j.jconrel.2022.10.011, PMID 36228953.
8. Tapfumaneyi P, Imran M, Mohammed Y, Roberts MS. Recent advances and future prospective of topical and transdermal delivery systems. Front Drug Deliv. 2022;2:957732. doi: 10.3389/fddev.2022.957732.
9. Abolmaali SS, Tamaddon AM, Farvadi FS, Daneshamuz S, Moghimi H. Pharmaceutical nanoemulsions and their potential topical and transdermal applications. Iran J Pharm Sci. 2011;7(3):139-50.
10. Tiwari G, Gupta M, Devhare LD, Tiwari R. Therapeutic and phytochemical properties of thymoquinone derived from *Nigella sativa*. Curr Drug Res Rev. 2024;16(2):145-56. doi: 10.2174/2589977515666230811092410, PMID 37605475.
11. Shabani H, Karami MH, Kolour J, Sayyahi Z, Parvin MA, Soghala S. Anticancer activity of thymoquinone against breast cancer cells: mechanisms of action and delivery approaches. Biomed Pharmacother. 2023;165:114972. doi: 10.1016/j.biopha.2023.114972, PMID 37481931.
12. Mohammed NK, Abd Manap MY, Tan CP, Muhialdin BJ, Alhelli AM, Meor Hussin AS. The effects of different extraction methods on antioxidant properties, chemical composition and thermal behavior of black seed (*Nigella sativa L.*) oil. Evid Based Complement Alternat Med. 2016;2016:6273817. doi: 10.1155/2016/6273817, PMID 27642353.
13. Yu F, Miao Y, Wang M, Liu Q, Yuan L, Geng R. Predicting nanoemulsion formulation and studying the synergism mechanism between surfactant and cosurfactant: a combined computational and experimental approach. Int J Pharm. 2022;615:121473. doi: 10.1016/j.ijpharm.2022.121473, PMID 35074435.
14. Chaudhari PM, Kuchekar MA. Development and evaluation of nanoemulsion as a carrier for topical delivery system by Box-Behnken design. Asian J Pharm Clin Res. 2018;11(8):286-93. doi: 10.22159/ajpcr.2018.v11i8.26359.
15. Sarheed O, Shouqair D, Ramesh KV, Khaleel T, Amin M, Boateng J. Formation of stable nanoemulsions by ultrasound-assisted two-step emulsification process for topical drug delivery: effect of oil phase composition and surfactant concentration and loratadine as ripening inhibitor. Int J Pharm. 2020;576:118952. doi: 10.1016/j.ijpharm.2019.118952, PMID 31843549.
16. Tinh NQ, Van Thanh D, Van Thu N, Quynh Nhung BT, Ngoc Huyen P, Phu Hung N. Preparation of nanoemulsions from *Elsholtzia kachinensis* and *Elsholtzia ciliata* essential oils via ultrasonic homogenization and their antibacterial and anticancer activities. RSC Adv. 2025;15(14):11243-56. doi: 10.1039/d5ra00386e, PMID 40206356.
17. Singh TP, Ahmad FJ, Jain GK, Verma N. Formulation development and characterization of nanoemulsion-based gel for topical application of raloxifene hydrochloride. Indian J Pharm Educ Res. 2021;55(4):996-1007. doi: 10.5530/ijper.55.4.200.
18. Azeem A, Rizwan M, Ahmad FJ, Iqbal Z, Khar RK, Aqil M. Nanoemulsion components screening and selection: a technical note. AAPS PharmSciTech. 2009;10(1):69-76. doi: 10.1208/s12249-008-9178-x, PMID 19148761.

19. International Conference on Harmonisation of Technical Requirements for Registration of Pharmaceuticals for Human Use (ICH). Q1A(R2): Stability Testing of New Drug Substances and Products. Geneva ICH; 2003.
20. Khadke R, Shete A, Dashawant A. Design and development of dasatinib nanoemulsions for ocular delivery: *in vitro* characterization, biocompatibility and ex vivo ocular irritation study. Int J Pharm. 2025;675:125504. doi: 10.1016/j.ijpharm.2025.125504, PMID 40132765.
21. Salmani JM, Asghar S, LV H, Zhou J. Aqueous solubility and degradation kinetics of the phytochemical anticancer thymoquinone; probing the effects of solvents pH and light. Molecules. 2014;19(5):5925-39. doi: 10.3390/molecules19055925, PMID 24815311.
22. Yu M, Yuan W, Li D, Schwendeman A, Schwendeman SP. Predicting drug release kinetics from nanocarriers inside dialysis bags. J Control Release. 2019;315:23-30. doi: 10.1016/j.jconrel.2019.09.016, PMID 31629038.
23. U.S. Food and Drug Administration. *In vitro* release test studies for topical drug products submitted in and as guidance for industry DRAFT GUIDANCE. Center for Drug Evaluation and Research; 2022. Available form: https://www.fda.gov/drugs/guidance-compliance-regulatory-information/guidances-drugs.
24. Suriyaamporn P, Kansom T, Charoenying T, Ngawhirunpat T, Rojanarata T, Patrojanasophon P. Computer-aided design and optimization of estradiol valerate nanoemulsion loaded core-shell microneedle patches for controlled release transdermal drug delivery. J Drug Deliv Sci Technol. 2024;95:105646. doi: 10.1016/j.jddst.2024.105646.
25. Hable AA, Jagdale SC, Chabukswar AR. Selection of optimum method for nanoparticles in lung cancer therapeutics. Biosci Biotech Res Asia. 2022;19(2):321-31. doi: 10.13005/bbra/2987.
26. Hawash M, Jaradat N, Qneibi M, Faraj HS, Rabi BM, Shalabi DZ. Antioxidant activity and neuromodulatory synergies in fixed oils from *Nigella sativa*, *Cucurbita pepo*, and *Sinapis alba* Seeds. Ind Crops Prod. 2025;228:120868. doi: 10.1016/j.indcrop.2025.120868.
27. Ramazi S, Salimian M, Allahverdi A, Kianamiri S, Abdolmaleki P. Synergistic cytotoxic effects of an extremely low-frequency electromagnetic field with doxorubicin on MCF-7 cell line. Sci Rep. 2023;13(1):8844. doi: 10.1038/s41598-023-35767-4, PMID 37258563.
28. Yadav PK, Saklani R, Tiwari AK, Verma S, Chauhan D, Yadav P. Ratiometric codelivery of paclitaxel and baicalein loaded nanoemulsion for enhancement of breast cancer treatment. Int J Pharm. 2023;643:123209. doi: 10.1016/j.ijpharm.2023.123209, PMID 37422142.
29. Zhang W, Liu J, Zhang Q, Li X, Yu S, Yang X. Enhanced cellular uptake and anti-proliferating effect of chitosan hydrochlorides modified genistein loaded NLC on human lens epithelial cells. Int J Pharm. 2014;471(1-2):118-26. doi: 10.1016/j.ijpharm.2014.05.030, PMID 24858387.
30. Bekhit M, Abu El Naga MN, Sokary R, Fahim RA, El Sawy NM. Radiation-induced synthesis of tween 80 stabilized silver nanoparticles for antibacterial applications. J Environ Sci Health A Tox Hazard Subst Environ Eng. 2020;55(10):1210-7. doi: 10.1080/10934529.2020.1784656, PMID 32614255.
31. Cho YH, Kim S, Bae EK, Mok CK, Park J. Formulation of a cosurfactant-free O/W microemulsion using nonionic surfactant mixtures. J Food Sci. 2008;73(3):E115-21. doi: 10.1111/j.1750-3841.2008.00688.x, PMID 18387105.
32. Hidayat AF, Fakih TM. Self-assembly of black cumin oil-based nanoemulsion on various surfactants: a molecular dynamics study. Makara J Sci. 2021;25(4):258-64. doi: 10.7454/mss.v25i4.1267.
33. Warisnoicharoen W, Lansley AB, Lawrence MJ. Nonionic oil-in-water microemulsions: the effect of oil type on phase behaviour. Int J Pharm. 2000;198(1):7-27, doi: 10.1016/S0378-5173(99)00406-8, PMID 10722947.
34. Piras A, Rosa A, Marongiu B, Porcedda S, Falconieri D, Dessi MA. Chemical composition and *in vitro* bioactivity of the volatile and fixed oils of *Nigella sativa L.* extracted by supercritical carbon dioxide. Ind Crops Prod. 2013;46:317-23. doi: 10.1016/j.indcrop.2013.02.013.
35. Periasamy VS, Athinarayanan J, Alshatwi AA. Anticancer activity of an ultrasonic nanoemulsion formulation of *Nigella sativa L.* essential oil on human breast cancer cells. Ultrason Sonochem. 2016;31:449-55. doi: 10.1016/j.ultsonch.2016.01.035, PMID 26964971.
36. Romes NB, Abdul Wahab R, Abdul Hamid M, Oyewusi HA, Huda N, Kobun R. Thermodynamic stability *in vitro* permeability and in silico molecular modeling of the optimal Elaeis guineensis leaves extract water-in-oil nanoemulsion. Sci Rep. 2021;11(1):20851. doi: 10.1038/s41598-021-00409-0, PMID 34675286.
37. Qushawy M, Mortagi Y, Alshaman R, Mokhtar HI, Hisham FA, Alattar A. Formulation and characterization of o/w nanoemulsions of hemp seed oil for protection from steatohepatitis: analysis of hepatic free fatty acids and oxidation markers. Pharmaceuticals (Basel). 2022;15(7):864. doi: 10.3390/ph15070864, PMID 35890162.
38. Liu W, Sun D, Li C, Liu Q, Xu J. Formation and stability of paraffin oil-in-water nano-emulsions prepared by the emulsion inversion point method. J Colloid Interface Sci. 2006;303(2):557-63. doi: 10.1016/j.jcis.2006.07.055, PMID 16905141.
39. Shah R, Gandhi J, Shah M, Tiwari P, Chaudhary B, Shah V. Nanoemulsions for topical delivery: formulation applications and recent advances. J Microencapsul. 2025;42(7):660-81. doi: 10.1080/02652048.2025.2531778, PMID 40694607.
40. Askarizadeh M, Esfandiari N, Honarvar B, Sajadian SA, Azdarpour A. Kinetic modeling to explain the release of medicine from drug delivery systems. ChemBioEng Rev. 2023;10(6):1006-49. doi: 10.1002/cben.202300027.
41. Lankanayaka A, Lakshan ND, Jayathunge L, Bandara P, Manatunga DC, Senanayake CM. A review of sustainable strategies for encapsulating antioxidant-rich plant polyphenolic extracts using nanoemulsification to enhance the oxidative stability of edible oils. Discov Food. 2025;5(1):65. doi: 10.1007/s44187-025-00331-8.
42. Medina Perez G, Estefes Duarte JA, Afanador Barajas LN, Fernandez Luqueno F, Zepeda Velasquez AP, Franco Fernandez MJ. Encapsulation preserves antioxidant and antidiabetic activities of cactus acid fruit bioactive compounds under simulated digestion conditions. Molecules. 2020;25(23):5736. doi: 10.3390/molecules25235736, PMID 33291808.
43. Tengku Din TA, Seeni A, Khairi WN, Shamsuddin S, Jaafar H. Effects of rapamycin on cell apoptosis in MCF-7 human breast cancer cells. Asian Pac J Cancer Prev. 2014;15(24):10659-63. doi: 10.7314/APJCP.2014.15.24.10659, PMID 25605156.
44. Mokhtary P, Javan B, Sharbatkhari M, Soltani A, Erfani Moghadam V. Cationic vesicles for efficient shRNA transfection in the MCF-7 breast cancer cell line. Int J Nanomedicine. 2018;13:7107-21. doi: 10.2147/IJN.S177674, PMID 30464462.
45. Chang NF, Tsai FJ, Zheng YM, Huang WH, Lin CC. Using a cellular system to directly assess the effects of cosmetic microemulsion encapsulated deoxyarbutin. Int J Mol Sci. 2021;22(23):13110. doi: 10.3390/ijms222313110, PMID 34884914.